SCIENCE CHINA
Chemistry

•ARTICLES•

June 2019 Vol.62 No.6: 732–738
https://doi.org/10.1007/s11426-018-9440-0

A facile design for multifunctional AIEgen based on tetraaniline derivatives

Beibei Liu[1], Wei He[2], Hao Lu[1], Kun Wang[1], Mingming Huang[1], Ryan Tsz Kin Kwok[2*], Jacky Wing Yip Lam[2], Longcheng Gao[3*], Jiping Yang[1*] & Benzhong Tang[2]

[1]*Key laboratory of Aerospace Advanced Materials and Performance, Ministry of Education, School of Materials Science and Engineering, Beihang University, Beijing 100191, China;*
[2]*Department of Chemistry, HKUST Jockey Club Institute for Advanced Study, Institute of Molecular Functional Materials, Division of Biomedical Engineering, State Key Laboratory of Molecular Neuroscience, Division of Life Science, The Hong Kong University of Science and Technology, Hong Kong, China;*
[3]*Laboratory of Bio-Inspired Smart Interfacial Science and Technology of Ministry of Education, Key Laboratory of Beijing Energy, School of Chemistry and Environment, Beihang University, Beijing 100191, China*

Received December 10, 2018; accepted February 12, 2019; published online March 27, 2019

Aniline oligomers have been widely used in many fields due to their excellent physicochemical properties. Owing to strong intermolecular interactions, their emission is always weakened or quenched when they are in high concentration or aggregated state, which greatly limits their fluorescent applications. Inspired by the concept of aggregation-induced emission (AIE), herein we introduced large steric groups onto the aniline oligomer to prevent the formation of packing structure. In particular, diphenyl vinyl group was bonded with oligomeric tetraaniline by a facile synthetic procedure with high yield. The obtained aniline oligomer derivative exhibited typical AIE features, which was also confirmed by density functional theoretical calculation. More importantly, this AIE oligomer was able to detect Fe^{3+} ions selectively and quantitatively. The fluorescence intensity decreased linearly along with the increment of Fe^{3+} concentration. Moreover, we demonstrated that this AIE oligomer could stain live bacteria, such as *E. coli* and *S. aureus* efficiently. All these results suggest that such a readily accessible and multifunctional tetraaniline derivative provides a new platform for the construction of fluorescent materials.

tetraaniline, aggregation-induced emission, Fe^{3+} ion detection, bacteria imaging

Citation: Liu B, He W, Lu H, Wang K, Huang M, Kwok RTK, Lam JWY, Gao L, Yang J, Tang B. A facile design for multifunctional AIEgen based on tetraaniline derivatives. *Sci China Chem*, 2019, 62: 732–738, https://doi.org/10.1007/s11426-018-9440-0

1 Introduction

Fluorescent materials have received intensive attention due to their rapid progress in various fields, such as organic light-emitting diodes, chemical and biological sensors, and fluorescent imaging [1–3]. However, fluorescent materials often present a fluorescence quenching phenomenon in aggregated state, which is so-called aggregation-caused quenching (ACQ). The emission intensity is weakened or even disappears under the condition of aggregation [4], which makes many potential molecules rejected by practical applications.

In 2001, Tang's group [5] coined a concept of aggregation-induced emission (AIE). When the molecules gathered together, their fluorescence was enhanced because of the restriction of intramolecular motions (RIM) mechanism [6,7]. Since then, great effort has been made on designing new AIE luminogens (AIEgens). A variety of AIE fluorophores have been developed, such as tetraphenylethene [8], siloles [9], pyrroles [10], and distyrylanthracene derivatives [11–13],

*Corresponding authors (email: chryan@ust.hk; lcgao@buaa.edu; jyang@buaa.edu)

and they have been applied in many fields such as fluorescence probes, bioimaging and mechano-fluorochromic materials [14–21]. However, traditional AIEgens are mainly synthesized by the McMurry reaction or lithium reaction [22,23] in somehow violent conditions or with limited yield.

On the other hand, aniline oligomers are cheap and easily prepared with special chain structure and excellent physical properties which make them a wide application prospect in electrochromic devices, electromagnetic shielding, metal anticorrosion and stealth technology [24–26]. However, most aniline oligomers suffer from the ACQ effect, for the reason that there exist different intermolecular interactions simultaneously, including π-π attractions, hydrophobic interactions, and hydrogen-bonding. Inspired by the AIE mechanism, introduction of steric groups onto the aniline oligomers could reduce the formation of packing structure, and thus it could be a solution for the ACQ problem.

Herein, a large diphenyl vinyl steric hindrance group was bonded with a tetraaniline in a simple synthetic route. The diphenyl vinyl groups worked as the aromatic rotors, preventing the destructive intermolecular π-π stacking interactions. In the solution state, the fluorescence emission of resulting tetraaniline derivative was weak but highly enhanced in the aggregated state, that is, the aniline oligomer with ACQ feature was transformed into AIE characteristics. Meanwhile, the new AIEgen possessed a highly fluorescence selectively towards Fe^{3+} for "turn-off" response and a "turn-on" bioimaging for bacteria. The AIE-type tetraaniline derivative could act as a new system for multifunctional AIE fluorophores with readily accessible synthesis and functionalization, which was encouraging for the development of novel fluorescent materials for scientific discoveries and technological innovations.

2 Experimental

2.1 Materials

4,4′-Diaminodiphenylamine sulfate hydrate and diphenylacetaldehyde was purchased from TCI Shanghai (China). 4-Fluoronitro-benzene was purchased from Innochem (China). Camphorsulfonic acid was purchased from Adamas (USA) and 10% Pd/C was from Acros (Belgium). Stock solutions containing metal ions of K^+, Na^+, Ca^{2+}, Mg^{2+}, Zn^{2+}, Mn^{2+}, Cd^{2+}, Co^{2+}, Cr^{3+}, Ni^{2+}, Pb^{2+}, Al^{3+}, Fe^{3+}, Eu^{3+}, Fe^{2+}, Ag^+ and Cu^{2+} were prepared in distilled water. Other reagents were purchased from Beijing Chemical Factory (China). All reagents and solvents were used without further purification.

2.2 Instruments

^{1}H NMR spectra were completed on a Bruker AV400 spectrometer (Germany) using deuterated dimethyl sulfoxide (DMSO-d_6) as solvent at 25 °C. Fourier transform infrared (FTIR) spectra were recorded on NEXUS-470 spectrometer (Nicolet, USA) using KBr pellet technique. UV-Vis absorption spectra were measured on a TU1901 UV-Vis spectrometer (Persee, China) at room temperature. MALDI-TOF MS measurements were carried out on Bruker Autoflex III SmartBeam (Germany). Fluorescence spectra were obtained using F-7000 fluorescence spectrophotometer (Hitachi, Japan). Laser confocal scanning microscopy images were collected on a Zeiss laser scanning confocal microscope (LSM7 DUO, Germany).

2.3 Synthesis

2.3.1 N,N-bis(4″-nitrophenyl)-4,4″-diaminodiphenylamine (NO_2-Ani_4-NO_2)

4,4′-Diaminodiphenylamine sulfate hydrate (9.22 g, 31 mmol) and triethylamine (9.95 g, 98 mmol) were dissolved in 50 mL of DMSO at room temperature, and 4-fluoro-nitrobenzene (11.03 g, 78 mmol) was added in sequence. The mixture was stirred at 90 °C for 72 h under nitrogen atmosphere to avoid amine oxidation. After the mixture was cooled to room temperature and poured into stirred water, the resulting precipitates were collected and purified by reprecipitation from tetrahydrofuran (THF) to give desired **NO_2-Ani_4-NO_2** as brown powder (11.62 g, yield 85%). FTIR (KBr, cm^{-1}): 3356 (N–H); 2975, 2913, 2848 (C–H, Ar); 1600, 1297 (NO_2); 1113 (C–N); 831, 750, 694 (C–H, Ar). ^{1}H NMR (400 MHz, DMSO-d_6), δ, ppm: 9.12 (s, 2H, C–NH), 8.22 (s, H, C–NH), 8.04 (d, 4H, Ar–H), 7.16–7.10 (m, 4H, Ar–H), 6.90 (d, 4H, Ar–H). MS (MALDI-TOF): *m*/*z*, 440.9 (M^+ calcd 441.1).

2.3.2 N,N″-bis[(4″-nitrophenyl)-N,N′,N″-tris(2,2-diphenyl-vinyl)-4,4′-diaminodiphenylamine (NO_2-B_3-Ani_4-NO_2)

NO_2-Ani_4-NO_2 (0.882 g, 2 mmol), camphorsulfonic acid (0.02 g, 0.08 mmol) and diphenyl acetaldehyde (1.177 g, 6 mmol) were dissolved in THF (30 mL), and the resulting mixture was heated to reflux for 24 h under nitrogen atmosphere with stirring. Then the solvent was removed by rotary evaporation, and the left crude product was purified by recrystallization from ethyl acetate (EA) to give **NO_2-B_3-Ani_4-NO_2** as red powder (1.70 g, yield 87%). FTIR (KBr, cm^{-1}): 3058, 2920, 2853 (C–H, Ar); 1586, 1311 (NO_2); 1502 (C=C); 1113 (C–N); 840, 750, 699 (C–H, Ar). ^{1}H NMR (400 MHz, DMSO-d_6), δ, ppm: 8.08 (d, 4H, Ar–H), 7.13–7.34 (m, 30H, Ar–H), 6.87 (d, 4H, Ar–H), 6.78 (d, 3H, CH=C), 6.55–6.60 (m, 8H, Ar–H). MS (MALDI-TOF): *m*/*z*, 975.3 (M^+ calcd 975.3).

2.3.3 N,N″-bis(4″-aminophenyl)-N,N′,N″-tris(2,2-diphenyl vinyl)-4,4′-diaminodiphenylamine (NH_2-B_3-Ani_4-NH_2)

NO_2-B_3-Ani_4-NO_2 (1.0 g, 1.02 mmol) and 10% Pd/C (0.1 g)

were dispersed into ethyl alcohol, and added into the three-neck flask with magnetic stirring under nitrogen atmosphere. Then 10 mL hydrazine hydrate was added dropwise into the flask. After it was stirred and refluxed for 24 h, the mixture was filtered to remove Pd/C, and then the filtrate was collected and cooled to room temperature to separate the product **NH_2-B_3-Ani_4-NH_2** as yellow powder after dried *in vacuo* at 50 °C (0.83 g, yield 89%). FTIR (KBr, cm^{-1}): 3291, 3045 (NH_2); 1500 (C=C); 1256 (C–N); 830, 764, 697 (C–H, Ar). ^{1}H NMR (400 MHz, DMSO-d_6), δ, ppm: 7.30–7.00 (m, 30H, Ar–H), 6.85 (s, 3H, CH=C), 6.57–6.40 (m, 16H), 4.84 (s, 4H, NH_2). MS (MALDI-TOF): *m*/*z*, 915.3 (M^+ calcd 915.4).

3 Results and discussion

3.1 Synthesis

For the aniline oligomers, e.g., trianiline and tetraaniline, their dilute *N*,*N*-dimethylformamide (DMF) solution showed strong luminescence. With gradual increase in the fraction of water, the emission became weakened, as shown in Figure S1 (Supporting Information online), presented typical ACQ feature. In order to hamper their intermolecular interactions, large steric groups, i.e. diphenyl vinyl groups, were introduced, considering both the function and ease of synthesis, as shown in Scheme 1. In detail, the nitro-capped tetraaniline derivative **NO_2-Ani_4-NO_2** was synthesized according to the references [24–26]. Then the nitro-capped diphenyl vinyl-substituted tetraaniline derivative **NO_2-B_3-Ani_4-NO_2** was synthesized by Schiff base reaction of secondary amine groups of **NO_2-Ani_4-NO_2** and aldehyde groups of diphenyl acetaldehyde. Finally, amino-capped tetraaniline derivative **NH_2-B_3-Ani_4-NH_2** was obtained by hydrazine hydrate Pd/C-catalytic reduction of **NO_2-B_3-Ani_4-NO_2**. The amino terminal groups enable the AIEgen additional functions, such as reaction points for condensation polymerization. The resulting products were obtained after easy purification, with relatively high yield and confirmed by FTIR, ^{1}H NMR and MALDI-TOF MS (presented in Figures S2–S4).

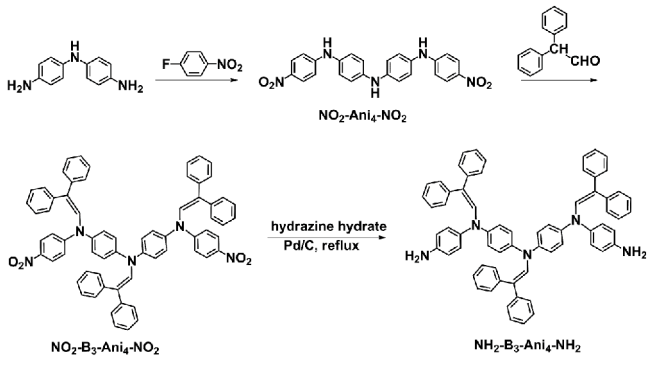

Scheme 1 Synthetic route of NH_2-B_3-Ani_4-NH_2.

The thermal behaviors of **NH_2-B_3-Ani_4-NH_2** were measured by thermogravimetric analysis (TGA) and differential scanning calorimeter (DSC), and depicted in Figure S5. The TGA curve displayed a high thermal stability of **NH_2-B_3-Ani_4-NH_2** with 5% weight loss occurring above 400 °C, while the DSC trace presented one peak at 231 °C which should be assigned to the melting temperature of **NH_2-B_3-Ani_4-NH_2**. All these results illustrated that **NH_2-B_3-Ani_4-NH_2** had a good thermal stability.

3.2 UV-Vis absorption and fluorescence emission spectra

The UV-Vis absorption and fluorescence emission spectra of **NH_2-B_3-Ani_4-NH_2** in different solvents were presented in Figure 1(a). Compared with its precursor **NH_2-Ani_4-NH_2** (Figure S6), the UV-Vis absorption and fluorescence emission peaks of **NH_2-B_3-Ani_4-NH_2** are red-shifted due to the contribution of diphenyl vinyl groups. Furthermore, two typical UV-Vis absorption bands at about 340 and 400 nm were presented which corresponded to π-π transitions of ethylene-phenyl conjugation structure and amino bonds, respectively. Meanwhile it gave similar absorption maxima in different solvents, indicating little change of dipole moments at its ground state in different solvents [21]. However, **NH_2-B_3-Ani_4-NH_2** exhibited weak emission in different solvents with solvent polarity dependence (Figure 1(b)). As illustrated in Table 1, the emission maximum was red-shifted from 494 to 534 nm and the band was broadened with increasing the solvent polarity from nonpolar toluene to polar DMF. The Stokes shift of **NH_2-B_3-Ani_4-NH_2** was increased with increased solvent polarity, producing a distinct maximum. These results were ascribed to the domination of intramolecular charge transfer (ICT) process.

3.3 AIE properties

The fluorescence spectra of **NH_2-B_3-Ani_4-NH_2** in DMF/H_2O mixture with concentration of 1.0 mM were presented in Figure 2(a)). Upon the excitation at 390 nm, **NH_2-B_3-Ani_4-NH_2** in pure DMF solvent exhibited weak emission at about 534 nm. When the water fraction (f_w) increased from 0% to 30%, the fluorescence intensity changed little. However, the fluorescence intensity of **NH_2-B_3-Ani_4-NH_2** was dramatically enhanced with increased f_w from 30% to 80%. The fluorescence intensity reached maximum at f_w=90%, which was 7.5-fold higher than that in the pure DMF solvent. This result confirmed that **NH_2-B_3-Ani_4-NH_2** was a typical AIE fluorophore.

Furthermore, the emission peak wavelength of **NH_2-B_3-Ani_4-NH_2** changed a little when the water was less than 30%, and then displayed hypsochromic shifted from 534 to 505 nm with the increase of non-solvent water up to 40%, as

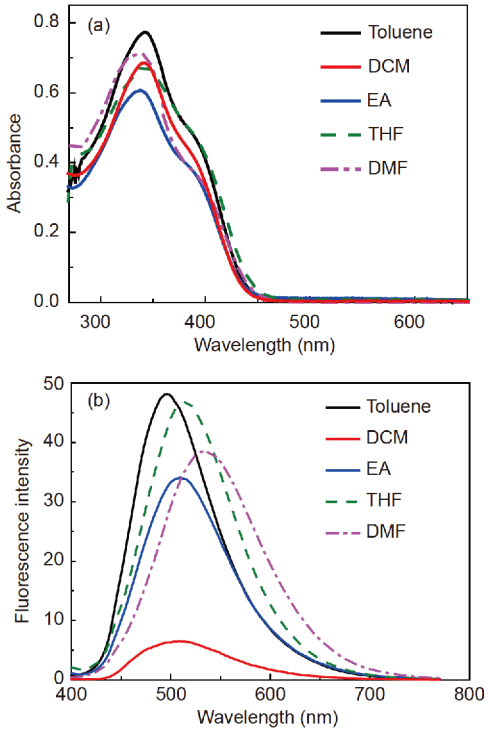

Figure 1 (a) UV-Vis absorption and (b) fluorescence spectra of **NH_2-B_3-Ani_4-NH_2** in different solvents. Concentration: 1.0 mM; excitation wavelength: 390 nm (color online).

Table 1 Photophysical properties of **NH_2-B_3-Ani_4-NH_2** in different solvents

Solvent	λ_{Abs} (nm)	λ_{FL} (nm)	Stokes shift (cm^{-1})
Toluene	343	494	8912
Dichloromethane	341	507	9602
EA	338	509	9939
THF	342	513	9747
DMF	338	534	10859

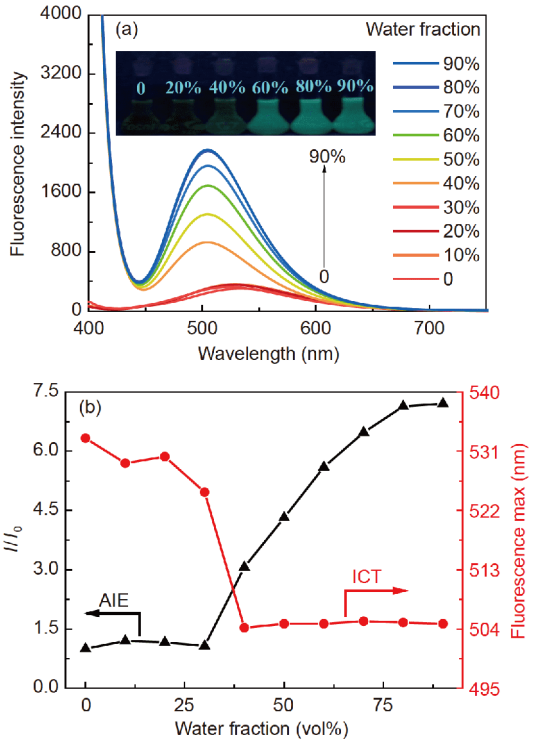

Figure 2 (a) Fluorescence spectra of **NH_2-B_3-Ani_4-NH_2** in DMF/H_2O mixture with different water fractions (inset: images of **NH_2-B_3-Ani_4-NH_2** in DMF/H_2O mixture with 0%–90% water content under 365 nm UV lamp); (b) plots of relative fluorescence intensity (I/I_0) and fluorescence maximum of **NH_2-B_3-Ani_4-NH_2** versus the water fraction in DMF/H_2O solution (I_0: fluorescence intensity of **NH_2-B_3-Ani_4-NH_2** in pure DMF; concentration: 1.0 mM; excitation wavelength: 390 nm) (color online).

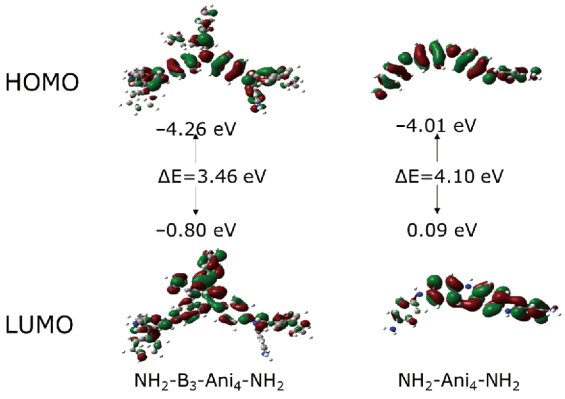

Figure 3 HOMO and LUMO spatial distributions of **NH_2-B_3-Ani_4-NH_2** and **NH_2-Ani_4-NH_2** (color online).

shown in Figure 2(b)). The hypsochromic shift was caused by the increased hydrophobicity of the local environment in the formed aggregates, which was consistent with the results in references [27–29]. As the aggregates have already formed, then the emission peak wavelength remained basically same (~505 nm) when the water fraction ranged from 40% to 90%.

For better understanding the AIE feature of the **NH_2-B_3-Ani_4-NH_2**, its electronic structures were theoretically calculated by density functional theory (DFT). The optimized molecular geometries and frontier orbitals were calculated and presented in Figure 3. The highest occupied molecular orbital (HOMO) was distributed on the chain backbone of tetraaniline motifs and partly localized on diphenyl vinyl groups. Because of the electron-donating amino group, the lowest unoccupied molecular orbital (LUMO) was mainly on the middle of diphenyl vinyl and tetraaniline part. Both HOMO and LUMO energy levels of AIEgen were more downshifted than that for its precursor **NH_2-Ani_4-NH_2**, owing to the contribution of diphenyl vinyl groups (−4.26 *vs.* −4.01 eV for HOMO, and −0.80 *vs.* 0.09 eV for LUMO of **NH_2-B_3-Ani_4-NH_2** and **NH_2-Ani_4-NH_2**, respectively). Based on the optimized structure, it was clear that the AIEgen adopted nonplanar conformation. The diphenyl vinyl groups were highly twisted out from aniline plane. These twisted

aromatic rotating units would serve as rotors to quench the fluorescence non-radiatively in the solution state, and prevent the molecules from detrimental π-π stacking in the aggregation, resulting in the AIE phenomenon [30,31].

3.4 Metal ion detection

To evaluate the possible metal ion detection capability of **NH_2-B_3-Ani_4-NH_2**, its luminescence behaviors in the DMF/H_2O solution were studied under different metal ion stimuli. The fluorescence responses of **NH_2-B_3-Ani_4-NH_2** to various cations, such as K^+, Na^+, Ca^{2+}, Mg^{2+}, Zn^{2+}, Mn^{2+}, Cd^{2+}, Co^{2+}, Cr^{3+}, Ni^{2+}, Pb^{2+}, Al^{3+}, Fe^{3+}, Eu^{3+}, Fe^{2+}, Ag^+ and Cu^{2+}, were examined under the same experimental condition. As shown in Figure 4(a, b), only Fe^{3+} induced an obvious fluorescence weakened under the given condition, indicating that this AIEgen was highly selective to Fe^{3+}, whereas other metal ions had no significant change in the emission intensity. In other word, **NH_2-B_3-Ani_4-NH_2** showed no response to the common anions, and its excellent Fe^{3+} selectivity implied its potential application for the sensing of Fe^{3+}. In addition, the fluorescence of **NH_2-B_3-Ani_4-NH_2** was decreased by Fe^{3+} but increased by Fe^{2+} at the same concentration (Figure 4(b)), suggesting **NH_2-B_3-Ani_4-NH_2** was also capable of differentiating Fe^{3+} and Fe^{2+}.

It is well known that Fe^{3+} is a necessary element for living organisms, which plays an essential role in metabolism and many enzyme reactions. The concentration of Fe^{3+} must be balanced in human body, and insufficient or excess Fe^{3+} may lead to a variety of illnesses such as anemia, diarrhea and hepatic cirrhosis [32,33]. Therefore, the Fe^{3+} ion detection ability of the AIEgen is valuable. Especially, this fluorescence detection technology is convenient, with low cost and high selectivity, which provides potential application in the Fe^{3+} detection [34,35].

In order to quantitatively evaluate the Fe^{3+} detection ability, the emission spectra of **NH_2-B_3-Ani_4-NH_2** solution mixed with different concentrations of Fe^{3+} were investigated (Figure 5(a)). The remarkable monotonic weakened fluorescence intensity was observed as the Fe^{3+} concentration increased. And the Stern-Volmer plot was constructed by applying Stern-Volmer equation (Eq. (1)) to understand Fe^{3+} quenching mechanism and the quenching efficiency, where I_0 and I were the original fluorescence intensity and quenched intensity in presence of the quencher [Fe^{3+}], and K_{SV} was the Stern-Volmer quenching constant.

$$\frac{I_0}{I} = 1 + K_{sv}[Fe^{3+}] \quad (1)$$

The K_{SV} value was 8.28×10^6 M^{-1} with the correlation coefficient (R^2) above 0.95 calculated from the plot of I_0/I values *versus* the concentrations of Fe^{3+} ions (Figure 5(b)). The higher value of K_{SV} indicated the efficient interaction between the Fe^{3+} ions and fluorophore. The deviation from

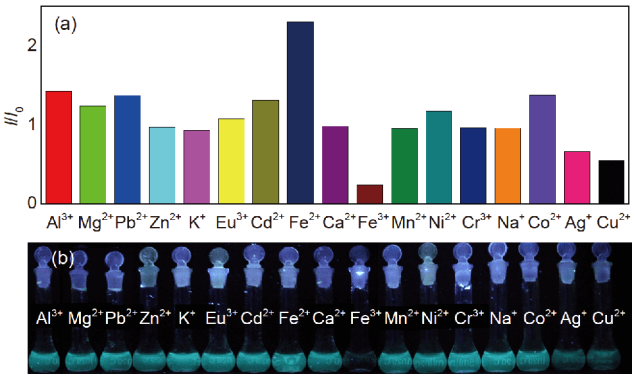

Figure 4 (a) The maximum fluorescence response of **NH_2-B_3-Ani_4-NH_2** (0.2 μM) upon the addition of different metal ions (0.2 μM) in DMF/H_2O (*v*/*v*=1:1) mixture; (b) fluorescence change induced upon the addition of 1.0 equiv. of various mental cations to **NH_2-B_3-Ani_4-NH_2** in DMF/H_2O (*v*/*v*=1:1) solution under 365 nm UV lamp (color online).

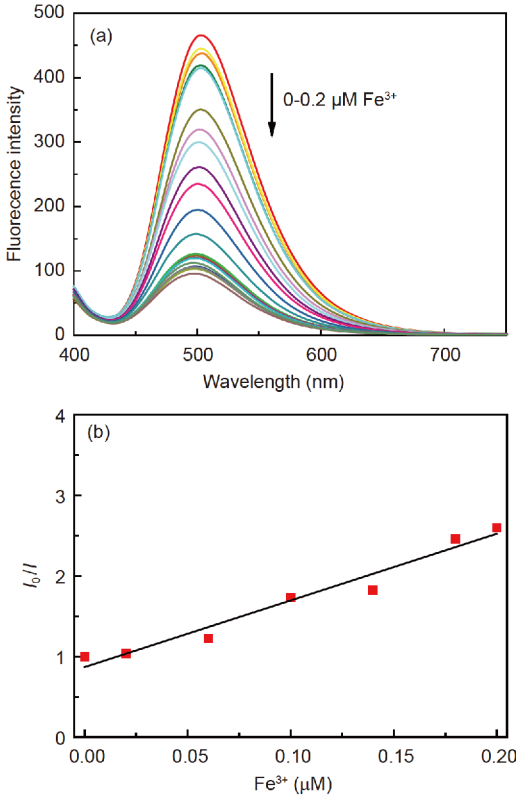

Figure 5 (a) Fluorescence spectra of **NH_2-B_3-Ani_4-NH_2** in DMF/H_2O (*v*/*v*=1:1, λ_{ex}=390 nm) with 0–0.2 μM of Fe^{3+}; (b) Stern-Vollmer plot for **NH_2-B_3-Ani_4-NH_2** at various contents of Fe^{3+} (0–0.2 μM) (color online).

the linearity of the plot with an upward curvature indicated a combination of the static and dynamic quenching mechanism for **NH_2-B_3-Ani_4-NH_2** [36–38].

Moreover, UV-Vis spectra were conducted to obtain more information on the binding form of sensor **NH_2-B_3-Ani_4-NH_2** with Fe^{3+}. As shown in Figure 6(a), **NH_2-B_3-Ani_4-NH_2** exhibited two absorption bands at about 340 and 400 nm. Upon the addition of Fe^{3+} to 1 equiv., the absorption band at

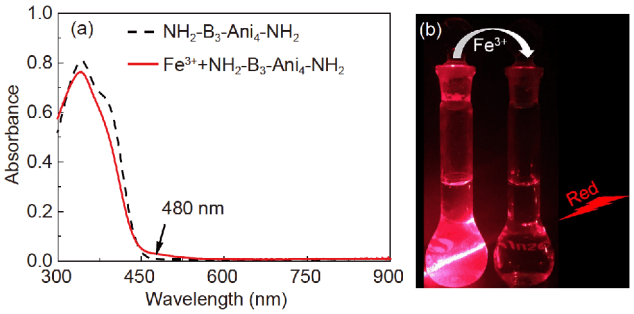

Figure 6 (a) UV-Vis spectra of 0.2 μM**NH_2-B_3-Ani$_4$-NH_2** and the **NH_2-B_3-Ani$_4$-NH_2** with the addition of Fe^{3+} (1 equiv.) in DMF/H_2O (v/v=1:1) solution; (b) photo image for the **NH_2-B_3-Ani$_4$-NH_2** suspension in DMF/H_2O with Tyndall effect and the **NH_2-B_3-Ani$_4$-NH_2** in DMF/H_2O without Tyndall effect after the addition of Fe^{3+} (color online).

~400 nm decreased obviously, and a new absorption band was developed at ~480 nm, indicating a weak interconversion between uncomplexed and complexed species had occurred [39]. **NH_2-B_3-Ani$_4$-NH_2** suspension in DMF/H_2O exhibited Tyndall effect (Figure 6(b)), while disappeared as Fe^{3+} was added, indicating that the aggregated AIEgen was gradually disaggregated. The intramolecular rotation was inspired, and sequentially the corresponding fluorescence intensity was reduced significantly. However, under the same conditions, no change occurred when other ions were added into the **NH_2-B_3-Ani$_4$-NH_2** suspension. The fluorescence intensity of diphenyl vinyl-substituted tetraaniline derivative without amino-capped group (**B_3-A_3**) did not change significantly as well in response to Fe^{3+} (Figure S7), indicating that fluorescence quenching of **NH_2-B_3-Ani$_4$-NH_2** induced by Fe^{3+} was due to the formation of interaction between amino and Fe^{3+}.

The binding stoichiometry of **NH_2-B_3-Ani$_4$-NH_2** and Fe^{3+} was determined by Job's method [40], in which the total concentration of two binding partners ([Fe^{3+}]+[**NH_2-B_3-Ani$_4$-NH_2**]) was remained constant, while their molar fraction was varied in the range of 0–0.8. As shown in Figure 7 (a), the change in Job's plot happened at [Fe^{3+}]/([Fe^{3+}]+[**NH_2-B_3-Ani$_4$-NH_2**])=0.3, implying that Fe^{3+} and **NH_2-B_3-Ani$_4$-NH_2** formed a complex with a molar ratio of 1:2, which resulted in the reduced AIE emission intensity in **NH_2-B_3-Ani$_4$-NH_2** aggregates, and the possible stoichiometry was shown in Figure 7(b).

3.5 Bacterial imaging

We further explored the application of the new AIEgen **NH_2-B_3-Ani$_4$-NH_2** in bacterial imaging. Because of the fluorescence "turn-on" characteristic upon aggregation, AIE probe could be used in bacterial imaging, which was important in the healthcare, food processing, and medical hygiene [41]. Two kinds of typical bacteria, Gram-negative *E. coli* and Gram-positive *S. aureus*, were detected. After incubation with the AIEgen (1.0 μM in DMSO) for 30 min without washing process, two kinds of bacteria were imaged under laser scanning confocal microscope using 405 nm laser and 410–585 nm emission filter. The clear fluorescence images of *E. coli* and *S. aureus* bacteria (Figure 8) indicated that the AIEgen could bind to *E. coli* and *S. aureus*. The possible reason should be that the AIEgen with positive charges was bound onto the negative charged bacteria cell wall based on the electrostatic interactions. Besides, the high fluorescence intensity should be attributed to the restriction of intramolecular motion induced by the trap of **NH_2-B_3-Ani$_4$-NH_2** in the bacterial walls or membranes [42,43]. It was also worth mentioning that **NH_2-B_3-Ani$_4$-NH_2** could image the bacteria with high fluorescence in a wash-free medium.

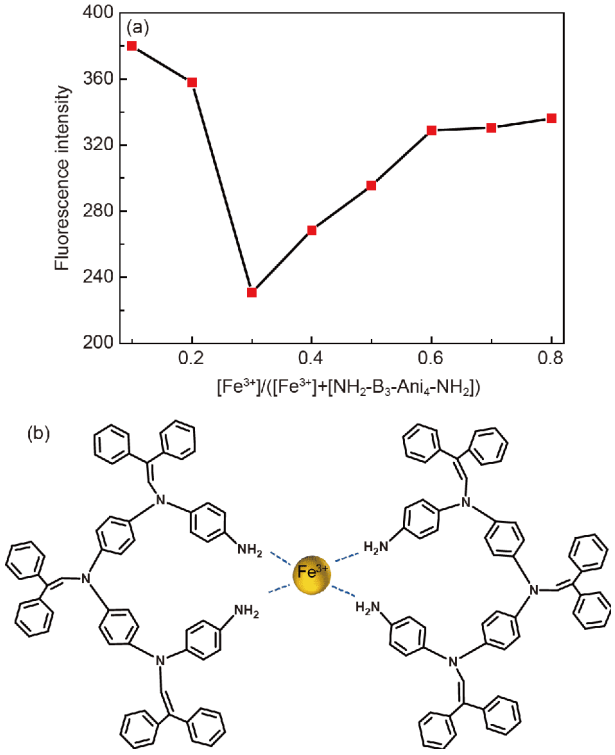

Figure 7 (a) Job's plot for **NH_2-B_3-Ani$_4$-NH_2** and Fe^{3+} system (the total concentration was 0.2 μM); (b) possible stoichiometry of **NH_2-B_3-Ani$_4$-NH_2** and Fe^{3+} complex (color online).

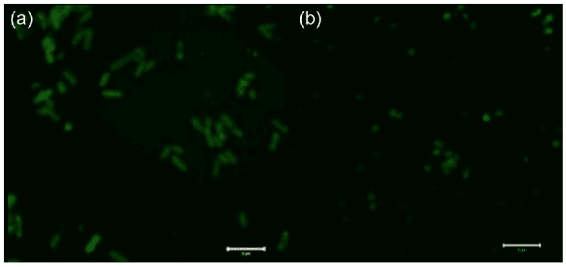

Figure 8 Confocal images of (a) *E. coli* and (b) *S. aureus* stained by **NH_2-B_3-Ani$_4$-NH_2**, respectively. Lasers: 405 nm; emission filter: 410–585 nm; scale bar: 5 μm (color online).

4 Conclusions

The amino-capped tetraaniline derivative **NH_2-B_3-Ani_4-NH_2** substituted with diphenyl vinyl groups was firstly designed and synthesized with high structural stability, large Stokes shift and high yield. The enhanced emission behavior in DMF/H_2O mixture with different water fractions indicated that **NH_2-B_3-Ani_4-NH_2** was a typical AIE fluorophore. Its optimized molecular geometries calculated by density functional theory confirmed that the restricted intramolecular rotation was the main reason for its AIE phenomenon. Importantly, the fluorescence intensity of **NH_2-B_3-Ani_4-NH_2** solution decreased with increased Fe^{3+} concentration, implying its capability for sensing of Fe^{3+}. Moreover, **NH_2-B_3-Ani_4-NH_2** could be used in the turn-on bioimaging for bacteria, i.e. *E. coli* and *S. aureus*. And these results suggested that the amino-capped tetraaniline derivative **NH_2-B_3-Ani_4-NH_2** could provide a new platform of AIE fluorophores for various high-tech applications.

Acknowledgements This work was supported by the National Natural Science Foundation of China (21574003, 21875009).

Conflict of interest The authors declare that they have no conflict of interest.

Supporting information The supporting information is available online at http://chem.scichina.com and http://link.springer.com/journal/11426. The supporting materials are published as submitted, without typesetting or editing. The responsibility for scientific accuracy and content remains entirely with the authors.

1 Liang J, Tang BZ, Liu B. *Chem Soc Rev*, 2015, 44: 2798–2811
2 Li Q, Li Z. *Sci China Chem*, 2015, 58: 1800–1809
3 Wang ZL, Ma K, Xu B, Li X, Tian WJ. *Sci China Chem*, 2013, 56: 1234–1238
4 Hong Y, Lam JWY, Tang BZ. *Chem Commun*, 2009, 1: 4332
5 Luo J, Xie Z, Lam JWY, Cheng L, Tang BZ, Chen H, Qiu C, Kwok HS, Zhan X, Liu Y, Zhu D. *Chem Commun*, 2001, 0: 1740–1741
6 Chen J, Law CCW, Lam JWY, Dong Y, Lo SMF, Williams ID, Zhu D, Tang BZ. *Chem Mater*, 2003, 15: 1535–1546
7 Hong Y, Lam JWY, Tang BZ. *Chem Soc Rev*, 2011, 40: 5361–5388
8 Dong Y, Lam JWY, Qin A, Liu J, Li Z, Tang BZ, Sun J, Kwok HS. *Appl Phys Lett*, 2007, 91: 011111
9 Zhao Z, He B, Tang BZ. *Chem Sci*, 2015, 6: 5347–5365
10 Li W, Chen D, Wang H, Luo S, Dong L, Zhang Y, Shi J, Tong B, Dong Y. *ACS Appl Mater Interfaces*, 2015, 7: 26094–26100
11 Li R, Xiao S, Li Y, Lin Q, Zhang R, Zhao J, Yang C, Zou K, Li D, Yi T. *Chem Sci*, 2014, 5: 3922–3928
12 Yang M, Zhang Y, Zhu W, Wang H, Huang J, Cheng L, Zhou H, Wu J, Tian Y. *J Mater Chem C*, 2015, 3: 1994–2002
13 Zheng M, Zhang DT, Sun MX, Li YP, Liu TL, Xue SF, Yang WJ. *J Mater Chem C*, 2014, 2: 1913–1920
14 Gu K, Qiu W, Guo Z, Yan C, Zhu S, Yao D, Shi P, Tian H, Zhu WH. *Chem Sci*, 2019, 10: 398–405
15 Shao A, Xie Y, Zhu S, Guo Z, Zhu S, Guo J, Shi P, James TD, Tian H, Zhu WH. *Angew Chem Int Ed*, 2015, 54: 7275–7280
16 Han T, Feng X, Tong B, Shi J, Chen L, Zhi J, Dong Y. *Chem Commun*, 2012, 48: 416–418
17 Song Y, Zong L, Zhang L, Li Z. *Sci China Chem*, 2017, 60: 1596–1601
18 Li Q, Li Z. *Adv Sci*, 2017, 4: 1600484
19 Chi Z, Zhang X, Xu B, Zhou X, Ma C, Zhang Y, Liu S, Xu J. *Chem Soc Rev*, 2012, 41: 3878–3896
20 Mei J, Huang Y, Tian H. *ACS Appl Mater Interfaces*, 2018, 10: 12217–12261
21 Qin A, Tang BZ. *Sci China Chem*, 2018, 61: 879–881
22 Zhao Z, Chen B, Geng J, Chang Z, Aparicio-Ixta L, Nie H, Goh CC, Ng LG, Qin A, Ramos-Ortiz G, Liu B, Tang BZ. *Part Part Syst Charact*, 2014, 31: 481–491
23 Song Z, Zhang W, Jiang M, Sung HHY, Kwok RTK, Nie H, Williams ID, Liu B, Tang BZ. *Adv Funct Mater*, 2016, 26: 824–832
24 Cao L, Gong C, Yang J. *Macromol Rapid Commun*, 2016, 37: 343–350
25 Huang LT, Yen HJ, Liou GS. *Macromolecules*, 2011, 44: 9595–9610
26 Cao L, Gong C, Yang J. *Electrochim Acta*, 2016, 192: 422–430
27 Wang E, Zhao E, Hong Y, Lam JWY, Tang BZ. *J Mater Chem B*, 2014, 2: 2013–2019
28 Kang M, Gu X, Kwok RTK, Leung CWT, Lam JWY, Li F, Tang BZ. *Chem Commun*, 2016, 52: 5957–5960
29 Jiang M, Gu X, Lam JWY, Zhang Y, Kwok RTK, Wong KS, Tang BZ. *Chem Sci*, 2017, 8: 5440–5446
30 Wen W, Shi ZF, Cao XP, Xu NS. *Dyes Pigments*, 2016, 132: 282–290
31 Shen XY, Wang YJ, Zhao E, Yuan WZ, Liu Y, Lu P, Qin A, Ma Y, Sun JZ, Tang BZ. *J Phys Chem C*, 2013, 117: 7334–7347
32 Pan C, Wang K, Ji S, Wang H, Li Z, He H, Huo Y. *RSC Adv*, 2017, 7: 36007–36014
33 Bian N, Chen Q, Qiu XL, Qi AD, Han BH. *New J Chem*, 2011, 35: 1667–1671
34 Kaya EN, Yuksel F, Özpınar GAı, Bulut M, Durmuş M. *Sens Actuators B-Chem*, 2014, 194: 377–388
35 Wang L, Li H, Cao D. *Sens Actuators B-Chem*, 2013, 181: 749–755
36 Niu Q, Sun T, Li T, Guo Z, Pang H. *Sens Actuators B-Chem*, 2018, 266: 730–743
37 Shi X, Wang H, Han T, Feng X, Tong B, Shi J, Zhi J, Dong Y. *J Mater Chem*, 2012, 22: 19296–19302
38 Wu WN, Mao PD, Wang Y, Mao XJ, Xu ZQ, Xu ZH, Zhao XL, Fan YC, Hou XF. *Sens Actuators B-Chem*, 2018, 258: 393–401
39 Pannipara M, Al-Sehemi AG, Kalam A, Asiri AM, Arshad MN. *Spectrochim Acta Part A-Mol Biomol Spectr*, 2017, 183: 84–89
40 He X, Wang X, Zhang L, Fang G, Liu J, Wang S. *Sens Actuators B-Chem*, 2018, 271: 289–299
41 Zhao E, Chen Y, Wang H, Chen S, Lam JWY, Leung CWT, Hong Y, Tang BZ. *ACS Appl Mater Interfaces*, 2015, 7: 7180–7188
42 Jiang G, Wang J, Yang Y, Zhang G, Liu Y, Lin H, Zhang G, Li Y, Fan X. *Biosens Bioelectron*, 2016, 85: 62–67
43 Zhou Y, Liu H, Zhao N, Wang Z, Michael MZ, Xie N, Tang BZ, Tang Y. *Sci China Chem*, 2018, 61: 892–897